Bone 66 (2014) 131–139

Contents lists available at ScienceDirect

Bone

journal homepage: www.elsevier.com/locate/bone

Technical Note

Characterization of cancellous and cortical bone strain in the in vivo mouse tibial loading model using microCT-based finite element analysis

Haisheng Yang [a], Kent D. Butz [b], Daniel Duffy [c], Glen L. Niebur [d], Eric A. Nauman [b,c], Russell P. Main [a,c,*]

[a] Musculoskeletal Biology and Mechanics Lab, Department of Basic Medical Sciences, Purdue University, IN, USA
[b] School of Mechanical Engineering, Purdue University, IN, USA
[c] Weldon School of Biomedical Engineering, Purdue University, IN, USA
[d] Department of Aerospace and Mechanical Engineering, University of Notre Dame, IN, USA

ARTICLE INFO

Article history:
Received 12 February 2014
Revised 29 May 2014
Accepted 30 May 2014
Available online 9 June 2014

Edited by: David Burr

Keywords:
In vivo compression loading
Mouse tibia
Bone adaptation
Cancellous strain
MicroCT finite element analysis

ABSTRACT

The in vivo mouse tibial loading model has been increasingly used to understand the mechanisms governing the mechanobiological responses of cancellous and cortical bone tissues to physical stimuli. Accurate characterization of the strain environment throughout the tibia is fundamental in relating localized mechanobiological processes to specific strain stimuli in the skeleton. MicroCT-based finite element analysis, together with diaphyseal strain gauge measures, was conducted to quantify the strain field in the tibiae of 16-wk-old female C57Bl/6 mice during in vivo dynamic compressive loading. Despite a strong correlation between the experimentally-measured and computationally-modeled strains at the gauge site, no correlations existed between the strain at the gauge site and the peak strains in the proximal cancellous and midshaft cortical bone, indicating the limitations of using a single diaphyseal strain gauge to estimate strain in the entire tibia. The peak compressive and tensile principal strain magnitudes in the proximal cancellous bone were 10% and 34% lower than those in the midshaft cortical bone. Sensitivity analyses showed that modeling bone tissue as a heterogeneous material had a strong effect on cancellous strain characterization while cortical strain and whole-bone stiffness were primarily affected by the presence of the fibula and the proximal boundary conditions. These results show that microCT-based finite element analysis combined with strain gauge measures provides detailed resolution of the tissue-level strain in both the cancellous and cortical bones of the mouse tibia during in vivo compression loading, which is necessary for interpreting localized patterns of modeling/remodeling and, potentially, gene and protein expression in skeletal mechanobiology studies.

Introduction

A critical relationship between physical load and adaptive remodeling in the skeleton has been formally postulated since Wolff, von Meyer, and Culmann related theoretical stress trajectories to cancellous bone architecture in the proximal human femur [1–3]. Since this time, it has been established that some stimulus related to the bone tissue strain environment is critical for initiating the (re)modeling response to applied load [4–7]. Recognition of this relationship places fundamental importance on the accurate characterization of the strain environment induced by applied load to understand the mechanisms governing the mechanobiological response of bone tissue to physical stimuli [8,9].

Experimental rodent models have been used to examine how controlled and repetitive loading modulates bone remodeling [10–15]. Development of the in vivo mouse tibial loading model provides the additional advantage of enabling the study of mechanobiological mechanisms in the metaphyseal corticocancellous and diaphyseal cortical tissues of the same bone [16–19]. Load-induced cortical strains in these models have been estimated using beam theory, surface strain gauge measures or surface digital image correlation [20,21]. Micro-computed tomography (microCT) based finite element (FE) analysis has been used more recently to quantify the strain field throughout the tibia [22–25]. However, most of these computational analyses focus on cortical bone and cancellous tissue strains are not well characterized. Furthermore, the FE model parameters applied in these previous studies varied, which may be at least partly responsible for differences in the strain distributions and magnitudes reported between studies. The effects of varying specific FE model parameters on strain predictions for the mouse tibia remain unclear.

The overall goal of this study was to characterize the strain environment in both cancellous and cortical bone for the in vivo mouse tibial loading model, using microCT-based FE analysis in combination with diaphyseal strain gauge measures. A series of sensitivity analyses were performed to first examine the contributions of specific model input

* Corresponding author at: Department of Basic Medical Sciences, 625 Harrison Street, West Lafayette, IN 47906, USA. Fax: +1 765 494 0781.
E-mail addresses: yang702@purdue.edu (H. Yang), kdbutz@purdue.com (K.D. Butz), duffdr01@gmail.edu (D. Duffy), gniebur@nd.edu (G.L. Niebur), enauman@purdue.edu (E.A. Nauman), rmain@purdue.edu (R.P. Main).

http://dx.doi.org/10.1016/j.bone.2014.05.019
8756-3282/

parameters to FE outcome measures. Based upon these analyses and the experimental boundary conditions determined for in vivo tibial loading, the strain environment throughout the entire tibia and whole-bone stiffness were subsequently quantified via the optimized FE models.

Materials and methods

Animals

Seven 16-wk-old female C57BL/6 mice were used in this study. The mice were obtained from a commercial vendor (Jackson Labs) and allowed to acclimate in our animal facility for one week prior to the experiments. During this time the mice had ad libitum access to water and commercial rodent diet and were maintained on a 12:12 light:dark cycle. At the start of the experiment, the mice weighed 20.7 ± 0.8 g. All experimental procedures were approved by Purdue University's Animal Care and Use Committee.

In vivo tibial loading and strain gauge measurements

Each mouse was anesthetized and, one leg at a time, an incision was made over the medial surface of the tibia. A single element strain gauge (EA-06-015LA-120, Micromeasurements) was aligned to the long axis of the bone and bonded to the medial surface of the tibial midshaft. Details of this surgical procedure were described previously [26,27].

While the mouse was anesthetized, the left and right hindlimbs were successively placed in custom-built foot and knee holders in a material testing device (TestBench, Bose) (Fig. 1A) [17,24,27,28] and maintained in place by a −1 N preload. Triangle waveform loads were applied at 4 Hz and characterized by 0.15 s of symmetric loading/unloading with a 0.10 s rest insertion between load cycles [17,27,28]. Four peak load levels were applied to each tibia (−3 N, −6 N, −9 N and −12 N) and the load and strain data recorded simultaneously at 2 kHz (LabChart, ADInstruments). The duration of each load trial was dependent upon the time required to reach repeatable peak strains (typically <30 s). Following data collection, the lead wires to the gauge were cut and the gauge was left intact on the bone. Mice were euthanized by carbon dioxide inhalation and the tibiae dissected free of soft tissue and stored in 70% ethanol at room temperature.

Four consecutive load cycles were chosen for each of the load levels tested to calculate the peak applied load-strain relationship at the gauge site [27]. For each mouse, a single load-strain relationship was calculated by averaging from the four load levels tested for both the left and right tibiae, where available. Four tibiae (from 4 mice) were excluded from subsequent analyses because (1) one mouse died while its right hindlimb was being loaded, but after the left tibia was tested, (2) two tibiae suffered broken fibulae during post mortem dissection, and (3) the strain gauge on one tibia detached from the bone prior to scanning by microCT.

MicroCT imaging

Intact tibiae with strain gauges attached to the bone surface were scanned in 70% ethanol using microCT (μCT 40, Scanco Medical AG). Prior to scanning, the solder leads on the strain gauges were removed using a scalpel. Batch scanning was performed for isotropic voxel resolutions of 10 μm and 20 μm (55 kVp, 145 mA, 300 ms integration time, no frame averaging). Scan times for each tibia at 10 μm and 20 μm resolutions were about 3.2 and 1.6 h, respectively. An aluminum filter was also used to reduce any beam hardening effects. No artifact was visible in the scans due to the attached strain gauges. A pre-set calibration was performed on the microCT scanner using a bone phantom (hydroxyapatite) provided by the manufacturer to convert attenuation values to bone mineral density (mg HA/cm^3).

Prior to analysis, all scans were aligned along the tibia's longitudinal axis using anatomical landmarks common to all mice [27]. The strain gauges were removed in the scans by omitting them from the bone contour using the Scanco software. Once aligned, volumes of interest (VOIs) for proximal cancellous bone and midshaft cortical bone were defined in each tibia [28]. The proximal cancellous VOI began approximately 0.5 mm distal to the proximal growth plate, excluding the primary spongiosa and cortical shell, and extended 10% of the total tibial length. The midshaft cortical VOI was centered at the middle of the diaphysis and spanned 2.5% of the total tibial length. Two threshold values (cancellous-based and cortical-based) for segmenting bone tissue were determined using the cancellous and cortical VOIs [24,29], respectively. The cancellous-based and cortical-based thresholds for all samples with a scan resolution of 10 μm were 197 ± 26 mg HA/cm^3

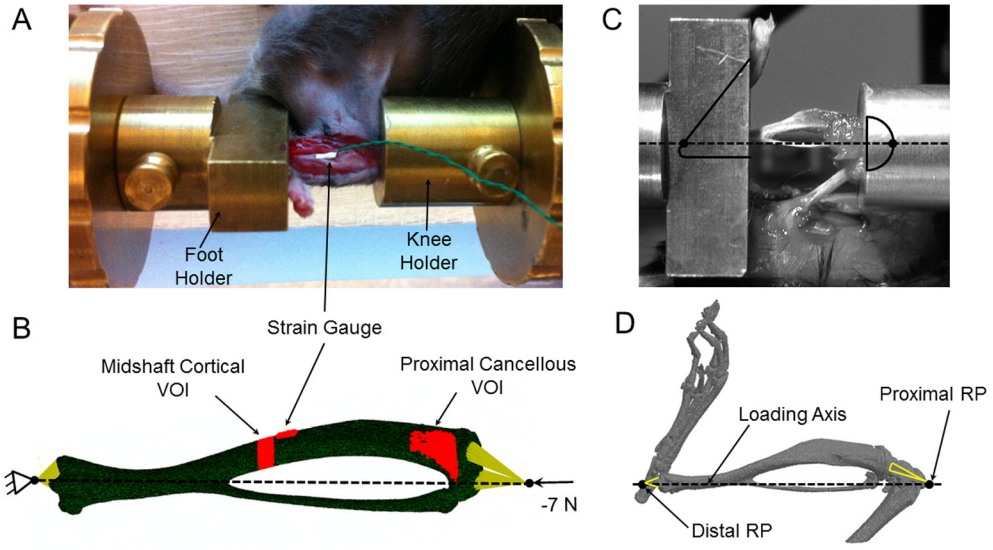

Fig. 1. (A) Experimental setup for the in vivo tibial strain measures. (B) A finite element model of a representative tibia showing the loading and boundary conditions for simulating the in vivo tibial loading experiment. The proximal cancellous and midshaft cortical volumes of interest (VOIs) and strain gauge site are highlighted in red. (C) The hindlimb skin and most of the muscles were removed in this cadaveric in situ preparation to show the alignment of the tibia relative to the knee and foot holders in the loading device. The dashed line connecting the central axes of the holders represents the loading axis through which the compressive force was applied. The knee and ankle joints were maintained intact. (D) The foot–tibia–femur complex was reconstructed from microCT scans. The proximal reference point (RP) was determined as the contact point (or a small area) between the knee cup and the peak of the patella. The distal RP was determined as the contact point between the calcaneus and foot holder in the loading axis.

(mean ± SD) and 371 ± 3 mg HA/cm^3, and with the scan resolution of 20 μm were 236 ± 40 mg HA/cm^3 and 400 ± 5 mg HA/cm^3, respectively.

Whereas the effect of using cortical-based vs. cancellous-based threshold values to segment the proximal cancellous bone in the tibia was examined in our sensitivity analyses (detailed below), the cancellous-based threshold was applied to the proximal fibula (~1.7 mm) for all specimens. This lower threshold value was required to mitigate the effects of structural discontinuities in the proximal fibular cortical bone that occurred when the cortical-based threshold was applied. The rest of the fibula and the tibia were segmented using the mean cortical-based threshold. The proximal cancellous bone and midshaft cortical bone were tagged with unique identifiers used later in the FE models.

MicroCT-based finite element modeling

The segmented microCT images for each tibial specimen were input into a Matlab-based mesh generation and processing program [30] to produce a three-dimensional FE mesh model consisting of tetrahedral elements. The mesh provided a smooth bone surface favorable for surface strain calculation, especially in the region of the strain gauge. The compartments of the proximal cancellous bone and midshaft cortical bone were identified in the FE model by the corresponding identifiers defined above (Fig. 1B). In the models, the exact location of the strain gauge was determined using the voxel coordinates from the original microCT scans in order to compare the simulated strains to the experimental strains measured at the gauge site.

The contact areas between the tibia and the distal femur and ankle/foot were identified using an ex vivo microCT scan of the foot–tibia–femur complex of a single intact hindlimb, with the limb positioned in the configuration maintained during in vivo loading (Figs. 1C and D). However, the limb was under no compressive load. The FE nodes at the contact surfaces on the tibial plateau (approximated as two ellipses with anterior–posterior and medial–lateral diameters of about 0.3 mm and 0.4 mm, respectively) were rigidly coupled to a proximal reference point (RP) and a −7 N load applied (Fig. 1B). This compressive load magnitude has been shown to induce anabolic responses in the proximal cancellous and midshaft cortical bone of the tibiae of female C57Bl/6 mice of similar age [31]. All nodes on the concave articular surface of the distal tibia were coupled to a distal RP where the boundary condition was applied (Fig. 1B). The bone elements between the RPs and the tibial contact surfaces (including the patella, distal femur, calcaneus, and astragulus) were excluded in the FE models (Fig. 1B).

Linear elastic FE analysis was performed in Abaqus 6.13.3 (Simulia) to simulate the in vivo tibial loading experiment. The strain environment throughout the whole bone, including the proximal cancellous and midshaft cortical bone, was characterized by the maximum and minimum principal and longitudinal strains. The cut-off values for the upper 95th percentile of those strains in each compartment were defined to represent the peak strains. The strain at the gauge site was calculated by averaging the nodal strains over the gauge zone in the

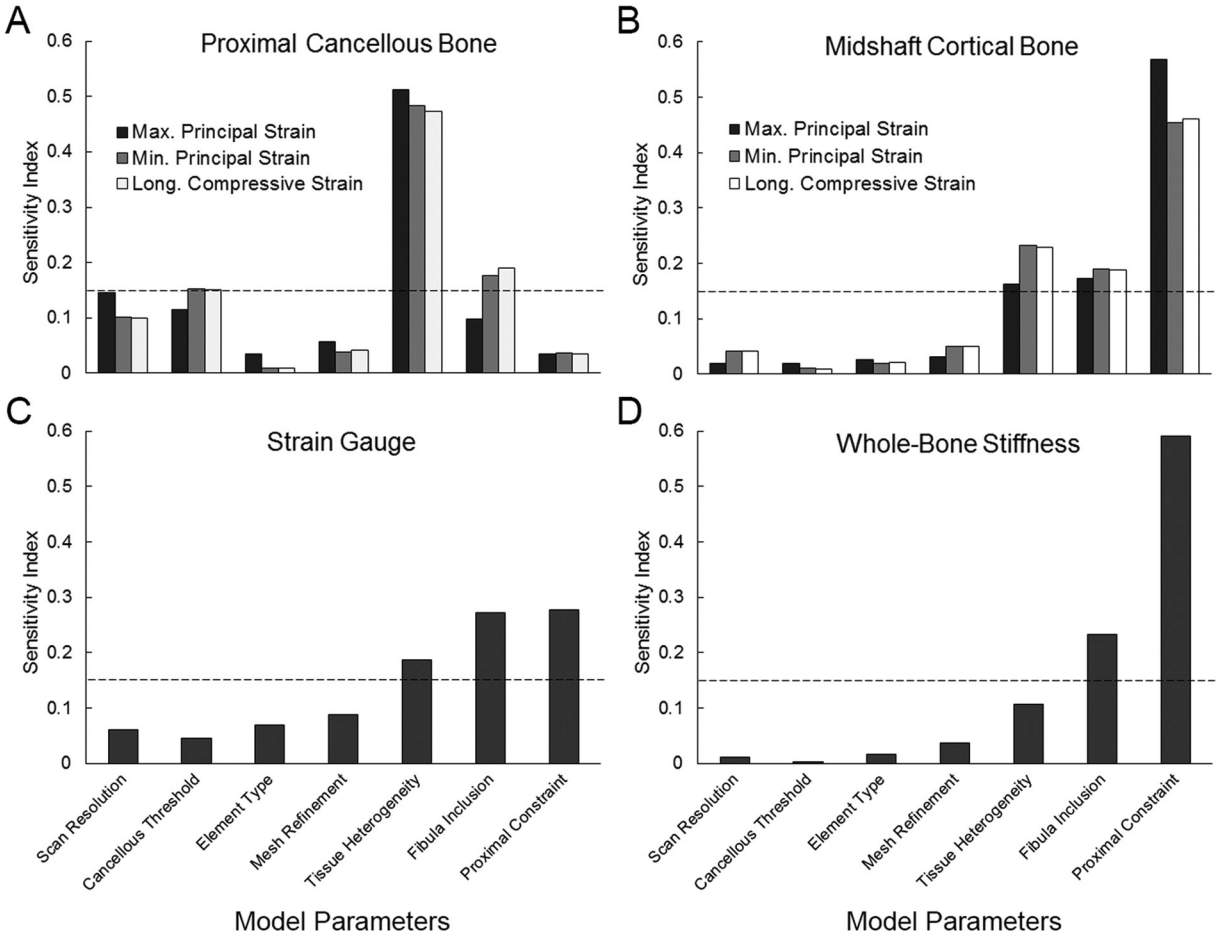

Fig. 2. Sensitivity indices resulting from a sensitivity analysis, including seven model parameters, for the peak (95th percentile) maximum principal strain, minimum principal strain and longitudinal compressive strain. (A) Proximal cancellous bone, (B) midshaft cortical bone, (C) strain at the strain gauge site and (D) whole-bone tibial stiffness. The dashed lines represent the null expectation that all parameters equally influence the model outcome. The 95th percentiles indicate the strain values that include elements within the top 5% for either cancellous or cortical bone.

longitudinal direction of the strain gauge. Whole-bone stiffness was defined as the compressive load over displacement along the loading axis.

Sensitivity analyses

Three sequential sensitivity analyses were performed on one representative tibia to examine the contributions of specific model parameters to FE analysis outcomes. The first two sensitivity analyses were conducted using Cotter's method and its essential features were described in detail elsewhere [32,33]. This approach required $2n + 2$ simulation trials for specified combinations of upper and lower levels for N model parameters [32]. Sensitivity indices were calculated to indicate the relative contribution of each model parameter to specific outcome measures of interest. In the final optimized models, parameters determined to have large effects on the model outcomes were chosen to most closely simulate our experimental conditions. Parameters determined to have little effect were chosen between the lower and upper values. Seven model parameters were evaluated in the first sensitivity analysis:

Scan resolution: Isotropic voxel resolutions of 10 μm and 20 μm were chosen as they have been commonly used for scanning mouse tibiae [24,34].
Cancellous threshold: We tested two threshold values (cancellous- or cortical-based) to segment the proximal cancellous bone.
Element type: 4-node linear and 10-node quadratic tetrahedral elements were tested.
Mesh refinement: Coarse and fine meshes of about 0.5 million and 3 million elements uniformly distributed throughout the entire tibial model were examined.
Tissue heterogeneity: Heterogeneous and homogeneous bone tissue material properties were evaluated. For the heterogeneous FE models, the tissue density for each bone element was mapped from the spatial distribution of tissue mineral density in the original microCT scans [35]. The elastic modulus was then calculated based upon a density-modulus relationship ($E = 1.127 \cdot 10^{-4}\rho^{1.746}$) [36], where tissue modulus (E) is in GPa and tissue mineral density (ρ) is in mg HA/cm^3. All bone elements were assigned a Poisson's ratio of 0.3 [37]. The heterogeneous material models had maximum, minimum and mean elastic modulus values of about 30 GPa, 2 GPa, and 15 GPa. The homogeneous models were assigned the mean elastic modulus for all bone elements.
Fibula inclusion: The fibula was either removed completely from the model or included and rigidly connected to the proximal tibia by filling the "gap" between them with elements of elastic modulus of 500 MPa. The latter was similar to the approach used in previous FE studies [25,37]. A "gap" was observed between the proximal ends of the tibia and fibula in the microCT scans because the two bones are capped with cartilage, which is radiographically transparent.
Proximal constraint: We set the proximal loading RP at the geometric center between the femoral condyle contact surfaces on the tibial plateau and then either allowed or completely restrained displacement of the proximal RP in the transverse plane perpendicular

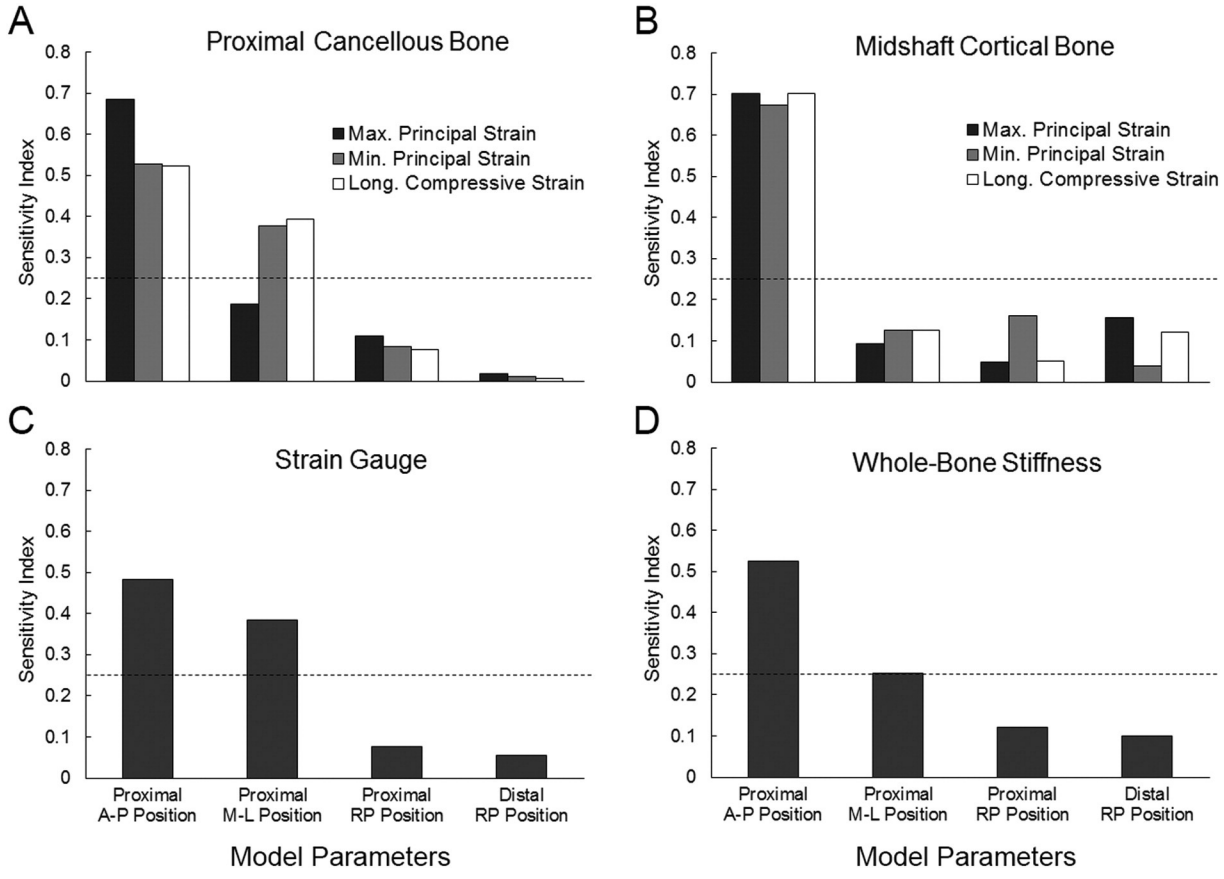

Fig. 3. Sensitivity indices resulting from a sensitivity analysis for the position of the loading reference point (RP) for the peak maximum principal strain, minimum principal strain and longitudinal compressive strain. (A) Proximal cancellous bone, (B) midshaft cortical bone, (C) strain at the strain gauge site and (D) whole-bone stiffness. The dashed lines represent the null expectation that all parameters equally influence the model outcome. A–P: anterior–posterior; M–L: medial–lateral. Model parameters: proximal A–P position (anterior-most vs. posterior-most); proximal M–L position (medial-most vs. lateral-most); proximal RP position (at bone surface vs. 3 mm proximal to the bone surface); distal RP position (at bone surface vs. 3 mm distal to the bone surface).

to the longitudinal axis of the tibia, representing two extreme cases for load application in the proximal tibia.

Based upon the results of the first sensitivity analysis, the three most influential model parameters were tissue heterogeneity, fibula inclusion and the proximal boundary condition. Thus, density-based heterogeneous material properties were used in subsequent analyses since they are specimen-specific. The "gap" elements bridging the space between the proximal tibia and fibula were assigned an elastic modulus of 0.5 MPa, representing realistic cartilage tissue [38]. The influence of the proximal and distal boundary conditions on model strain predictions was examined further by conducting two additional sensitivity analyses. The second sensitivity analysis evaluated the contributions of positional changes in the proximal and distal RPs to tibial strain environment. The third sensitivity analysis was performed to understand the influence of fine-scale changes in the anterior–posterior and medial–lateral positions of the proximal RP on the modeled bone strain magnitudes.

Ultimately the locations of the proximal and distal RPs were determined based upon digital measures of the limb comformation in our specific experimental setup (Figs. 1C and D). Axial displacement of the proximal RP was allowed in order to simulate the compression-actuated motion along the loading axis. Since the foot conforms to the slot in the distal holder and the tarsals and distal tibia articulate closely in the joint (Fig. 1A), the distal RP was constrained against displacement in all directions and rotation about the longitudinal loading axis. The simulated results for strain at the gauge site, peak strains in the cancellous and cortical volumes, and whole-bone stiffness were determined and related to gauge-based strains determined by the experimental load-strain relationship at a −7 N load.

Results

The first sensitivity analysis showed that modeling bone tissue as a heterogeneous material had a strong effect on the simulated cancellous strains compared to applying homogeneous material properties to this tissue (Fig. 2A). Minor influences on cancellous strains were observed for scan resolution, cancellous tissue threshold, and inclusion of the fibula in the model (Fig. 2A). Strains in the midshaft cortical bone, the strain at the gauge site and the stiffness of the whole tibia were primarily affected by the proximal boundary condition, and influenced to a lesser degree by the tissue heterogeneity and inclusion of the fibula in the model (Figs. 2B, C and D).

The second sensitivity analysis demonstrated that the strains in both the proximal cancellous bone and midshaft cortical bone and whole-bone stiffness were mainly affected by the anterior–posterior and

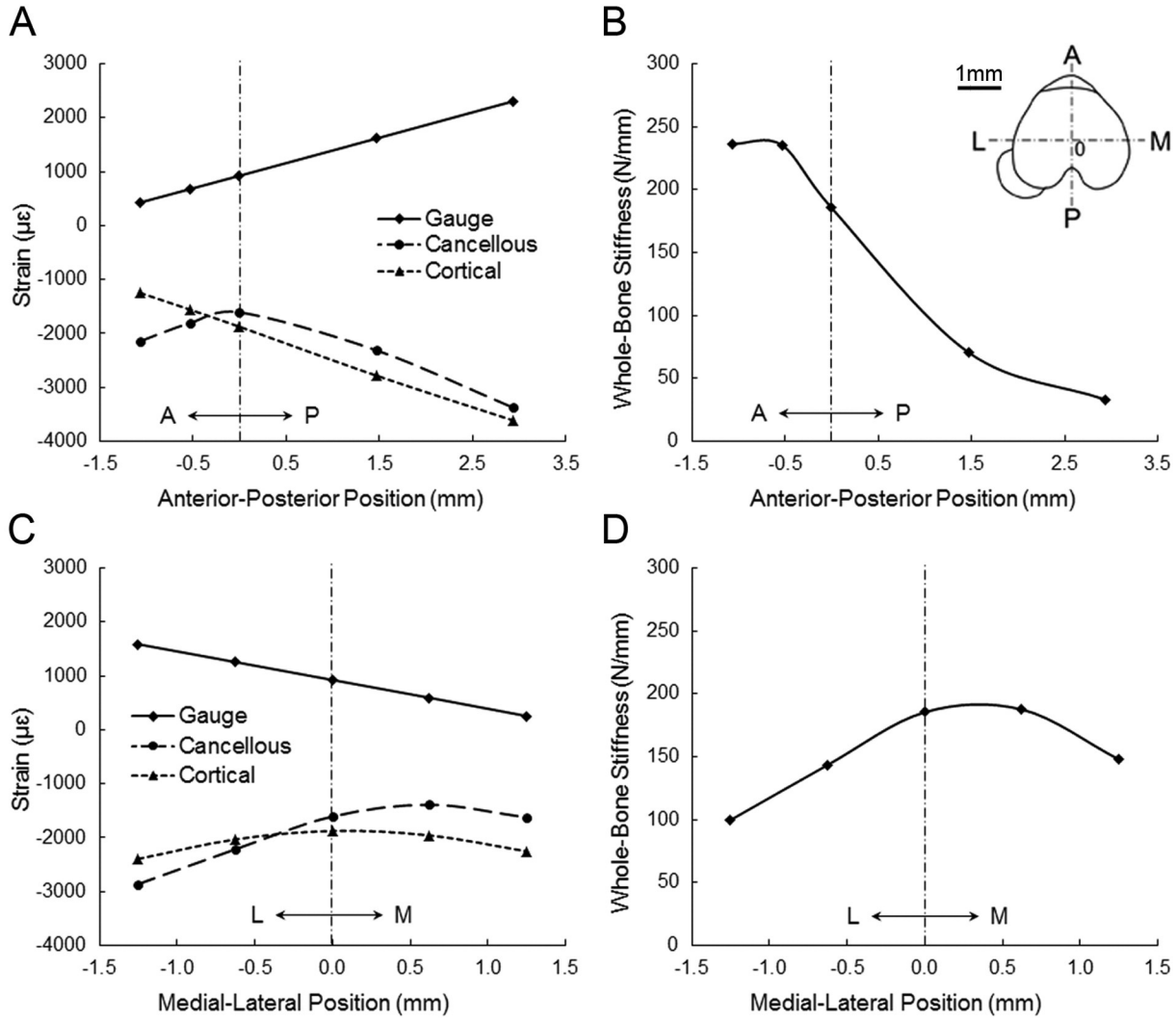

Fig. 4. Variation in strain values for the cancellous and cortical volumes of interest, the strain gauge, and whole-bone stiffness when the position of the proximal loading reference point was varied in the anterior–posterior (A, B) or medial–lateral directions (C, D). The strain values for the cancellous and cortical bone are presented as the peak minimum principal strains. The trend lines presented are best-fit lines.

medial–lateral positions of the proximal RP (Fig. 3). A 1 mm shift of the proximal loading RP in the transverse plane from anterior to posterior (or from medial to lateral) led to an increase in strain magnitude of about 500 με at the gauge site (Fig. 4), as a result of increased diaphyseal bending. Strain magnitudes in the cancellous and cortical bone and whole-bone stiffness were also sensitive to variation in the position of the proximal loading RP (Fig. 4), with the exception of medial–lateral RP position on mid-diaphyseal cortical strain (Fig. 4C).

The experimentally-measured strain values correlated very closely to the computationally-modeled strain values at the gauge site (slope: 1.01, $R^2 = 0.66$, Fig. 5A). Conversely, no correlations were found between the measured strain at the gauge site and the modeled strains in the proximal cancellous bone, the midshaft cortical bone, or the modeled whole-bone stiffness (Figs. 5B, C and D). The measured strains at the gauge site induced by a −7 N load varied across a relatively large range (mean ± SD = 1388 ± 210 με, coefficient of variation (CV) = 0.15), while the modeled strains in the cancellous and, especially, the cortical bone and whole-bone stiffness exhibited less variation across the specimens (Fig. 5, Table 1). The peak longitudinal compressive strains and minimum principal strains in the midshaft cortical bone were about twice the absolute magnitude of the measured strains at the gauge site (2.1 ± 0.3, $p < 0.001$ paired *t*-test).

The strain distribution in the whole tibia showed that the greatest compression and tension occurred at the posterior and anterior surfaces of the midshaft, respectively, and shifted to the posterior-lateral and anterior-medial aspects in the proximal diaphysis (Fig. 6). The posterior

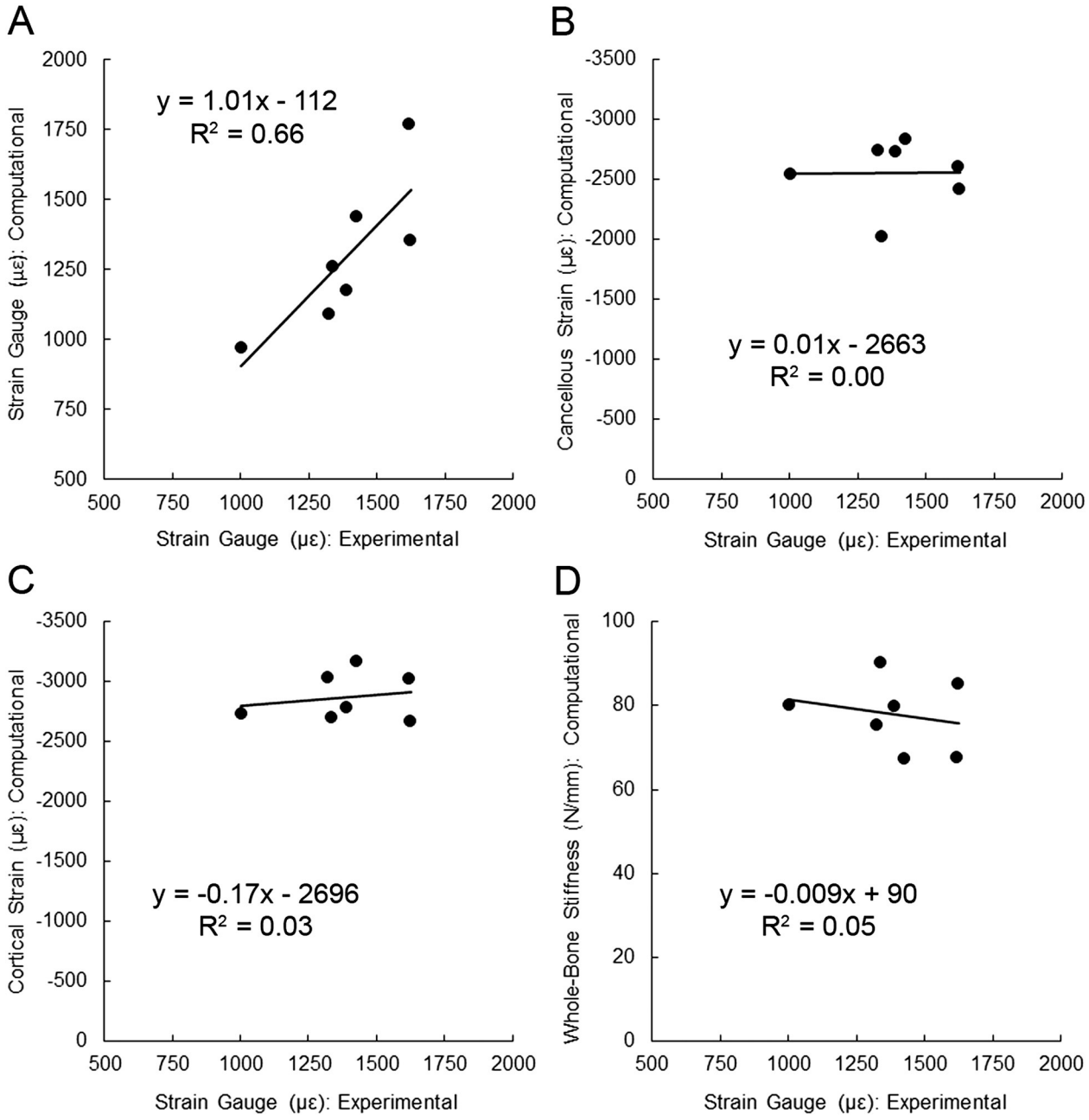

Fig. 5. Relationships between the experimentally-measured strain at the medial midshaft gauge site and computationally-simulated (A) strain at the strain gauge, (B) peak minimum principal strain in the proximal cancellous bone, (C) peak minimum principal strain in the midshaft cortical bone and (D) whole-bone stiffness. Specific model parameters for the optimized FE models used here include: 10 μm scan resolution, cancellous-based threshold for the proximal cancellous bone tissue, about 1.5 million 4-node tetrahedral elements, density-based heterogeneous material properties, fibula present and connected to the tibia through cartilage-like tissue, and the locations of the proximal and distal RPs determined based upon our specific experimental configuration.

Table 1
Strains in the proximal cancellous and midshaft cortical volumes of interest for 16-wk-old female C57BL/6 mouse tibiae under an axial compressive load of 7 N.

	Proximal cancellous bone		Midshaft cortical bone	
	Mean (±SD)	CV	Mean (±SD)	CV
Maximum principal strain				
95th percentile	1705 (±240)[a]	0.14	2588 (±233)	0.09
Average	675 (±80)[a]	0.12	1008 (±88)	0.09
Minimum principal strain				
95th percentile	−2644 (±319)[b]	0.12	−2939 (±208)	0.07
Average	−993 (±108)[a]	0.11	−1277 (±99)	0.08
Longitudinal strain				
95th percentile (tens)	662 (±157)[a]	0.24	2356 (±205)	0.09
95th percentile (comp)	−2277 (±274)[a]	0.12	−2870 (±199)	0.07
Average	−594 (±57)[a]	0.10	−418 (±29)	0.07

Data are presented as means (±SD) and coefficient of variation (CV) for 7 mice.
The 95th percentiles indicate the cutoff strain values that include elements within the top 5% for either cancellous or cortical bone.
[a] $p < 0.0001$ vs. midshaft cortical bone, by paired *t*-test.
[b] $p < 0.05$ vs. midshaft cortical bone.

cancellous bone of the proximal metaphysis was highly compressed, while the anterior cancellous bone experienced relatively low-magnitude tension (Fig. 6). The peak minimum and maximum principal strain values in the proximal cancellous bone were 10% and 34% lower than those in the midshaft cortical bone, respectively (Table 1).

Discussion

The overall goal of this study was to characterize the strain environment in the cancellous and cortical bone of the mouse tibia during in vivo axial compression loading. A strong correlation between modeled and experimentally-measured strains at the gauge site validates the robustness of our general model. Our FE analyses showed that the peak compressive and tensile principal strains in the proximal cancellous bone were 10% and 34% lower than those in the midshaft cortical bone, respectively. The sensitivity analyses demonstrated that modeling bone tissue as a heterogeneous material had a strong influence on cancellous strain characterization in the proximal metaphysis, while cortical strain in the midshaft was mainly affected by the presence of the fibula and the boundary conditions at the proximal end of the tibia.

Despite a strong correlation between the experimentally-measured and computationally-modeled strains at the gauge site, there were no correlations between the gauge-measured strains and peak strains in the proximal cancellous and midshaft cortical bone. Prior in vivo tibial loading studies usually perform single gauge measures to calibrate the applied loads needed to induce a chosen target strain at the medial surface of the tibial midshaft [16–18,28]. However, we show here that the gauge-measured strains did not closely reflect the peak tensile or compressive strains in the tibia, even in the midshaft cortical bone. The lack of correlation between the gauge-measured strains and peak strains is likely due to variation in gauge location between specimens. Measures from the microCT scans showed that the center of the gauge element ranged in position from 0.63 mm to 1.23 mm proximal to the midshaft (CV = 0.24) and 0.25 mm to 0.46 mm posterior to the anterior edge of the diaphysis (CV = 0.17) across all specimens. Because the strain gauge location on the medial tibia is near the neutral axis, where a strong gradient from compression to tension occurs (Fig. 6), even these very small differences in gauge position can cause large variation in measured strains between specimens [39].

The compression-induced strains in the proximal cancellous bone of the tibia were lower than the strains in the midshaft cortical bone. A recent tibial loading study that applied successively greater loads (5 N, 7 N, 9 N) to the tibiae of 16-wk-old female C57BL/6 mice reported no trabecular bone response until the applied load reached 9 N, in contrast

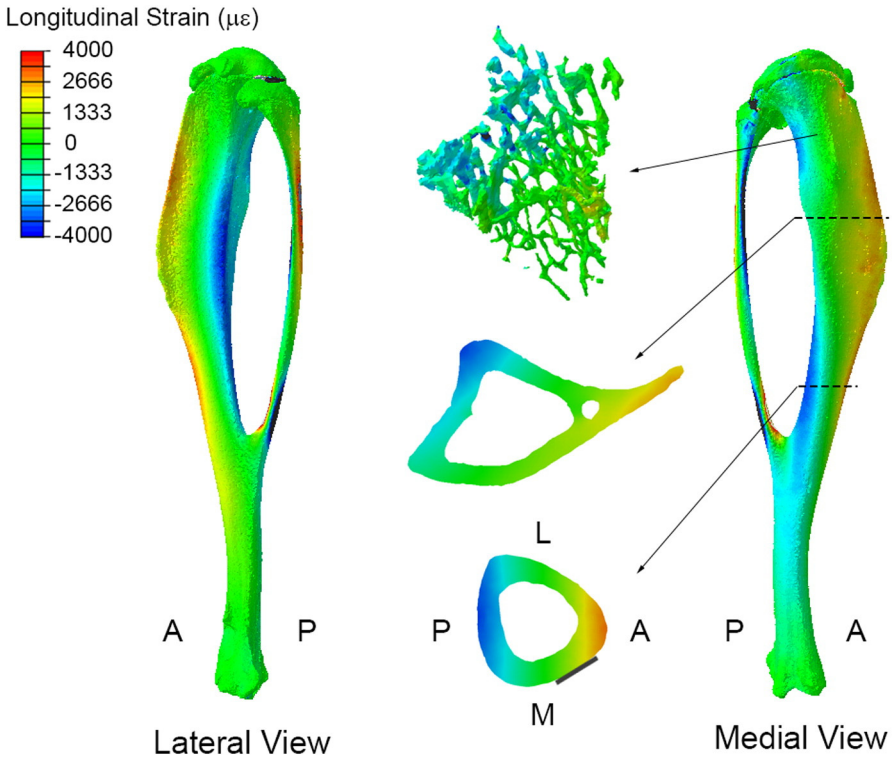

Fig. 6. Distribution of longitudinal strains in a representative tibia in the proximal cancellous volume of interest, the proximal cortex (25% of the bone's length from the proximal articular surface) and midshaft cortex. Red and blue indicate longitudinal tension and compression, respectively. The gauge position in the cross-section of the midshaft is indicated by a black rectangle. A = anterior, P = posterior, M = medial, L = lateral.

to an incremental anabolic cortical bone response at the midshaft with increasing load magnitudes between 5 N and 9 N [18]. Whether the strain thresholds are similar for stimulating bone formation in cortical and cancellous bone tissues remains unclear due to a lack of data for cancellous strains induced by tibial compression loading. Based upon our results, however, the lower magnitude strains induced in the proximal cancellous bone, compared to the midshaft cortical bone, could provide rationale for the lack of response observed for cancellous tissues to the low-magnitude loads that were anabolic in diaphyseal cortical tissue.

Our sensitivity analyses could provide some insight regarding the causes for variation in the strain environments reported in different tibial loading FE studies. In prior studies, the ratio of the peak modeled compressive to tensile strains in diaphyseal cortical bone varied considerably from about 1.5 to 3 [23–25], indicating a relative shift in the estimated position of the diaphyseal neutral axis of bending between the different studies. According to our sensitivity analyses, such inconsistencies could most likely be due to variation in the position of the proximal loading point, which would influence the amount of bending induced in the tibial diaphysis. The peak longitudinal compressive strains in the cancellous bone of a single 19-wk-old female C57BL/6 mouse tibia reported in a recent study [23] were about one third of the peak longitudinal compressive strains reported here, at the same load magnitude. The cancellous bone tissue was modeled as a homogeneous material in the prior study (17 GPa) and a heterogeneous material in our study (Mean: ~15 GPa, Range: ~2 GPa to ~30 GPa), which likely explains the difference in resulting peak cancellous strain magnitudes.

There are several limitations to the current implementation of our FE technique. First, only static linear elastic FE analyses were performed to characterize the strain magnitude and distribution in the mouse tibia at a peak load. To understand the mechanisms underlying skeletal adaptation to mechanical stimuli, time-varying factors related to dynamic features of the applied loading (e.g. strain rate, load frequency) must also be considered [6,7]. Additionally, the influence of soft tissues in the knee and ankle joints, including cartilage and ligaments, was neglected in our FE simulations. We expect exclusion of these tissues to have a minimal effect on the peak load-induced strain environment in the tibia because the viscoelasticity inherent in these tissues might only casue a delay in the timing of the peak strains [40]. Lastly, the mathematical relationship we used to relate bone tissue mineral density to elastic modulus in the FE models was not obtained through direct mechanical testing of the bone specimens used in this study. Instead, this relationship was determined previously for a comprehensive sample of vertebrate species, including human and rodent bone samples [36], which likely adequately represents the range of tissue mineral densities measured in the mouse tibiae included in this study.

In summary, a combination of strain gauge measures and microCT-based FE analysis allows for validated quantification of the tissue-level strain in both cancellous and cortical bone in the in vivo mouse tibial loading model. The use of a single strain gauge measure to characterize the strain environment within the entire tibia may be inadequate. Peak compressive and tensile strains in the proximal cancellous bone of the tibia caused by axial compression loading are lower in magnitude than the strains induced in the midshaft cortical bone. Accurate characterization of the strain environment within the mouse tibia using microCT-based FE analysis should include modeling the bone tissues as a heterogeneous material and incorporate experiment-specific boundary conditions.

Acknowledgments

This work was supported by the Ralph W. and Grace M. Showalter Research Trust (RPM), a Purdue SURF fellowship (DD) and a Purdue Research Foundation Summer Faculty Grant (RPM). We thank the Purdue Bone and Body Composition Core of the Indiana CTSI for providing micro-CT scanning. We are grateful to Dr. Bettina Willie (Julius Wolff Institute For Biomechanics and Musculoskeletal Regeneration, Berlin) for sharing with us the designs for the loading device fixtures.

References

[1] Wolff J. The Law of Bone Remodelling. Berlin; New York: Springer-Verlag; 1986.
[2] Roesler H. The history of some fundamental concepts in bone biomechanics. J Biomech 1987;20:1025–34.
[3] Cowin S. Bone Mechanics Handbook. 2nd ed. Boca Raton: CRC Press; 2001.
[4] Lanyon LE. Functional strain in bone tissue as an objective, and controlling stimulus for adaptive bone remodelling. J Biomech 1987;20:1083–93.
[5] Gross TS, Edwards JL, McLeod KJ, Rubin CT. Strain gradients correlate with sites of periosteal bone formation. J Bone Miner Res 1997;12:982–8.
[6] Turner CH. Three rules for bone adaptation to mechanical stimuli. Bone 1998;23:399–407.
[7] Burr DB, Robling AG, Turner CH. Effects of biomechanical stress on bones in animals. Bone 2002;30:781–6.
[8] Carter DR. The relationship between in vivo strains and cortical bone remodeling. Crit Rev Biomed Eng 1982;8:1–28.
[9] Frost HM. Bone's mechanostat: a 2003 update. Anat Rec A Discov Mol Cell Evol Biol 2003;275:1081–101.
[10] Turner CH, Akhter MP, Raab DM, Kimmel DB, Recker RR. A noninvasive, in vivo model for studying strain adaptive bone modeling. Bone 1991;12:73–9.
[11] Torrance AG, Mosley JR, Suswillo RF, Lanyon LE. Noninvasive loading of the rat ulna in vivo induces a strain-related modeling response uncomplicated by trauma or periostal pressure. Calcif Tissue Int 1994;54:241–7.
[12] Gross TS, Srinivasan S, Liu CC, Clemens TL, Bain SD. Noninvasive loading of the murine tibia: an in vivo model for the study of mechanotransduction. J Bone Miner Res 2002;17:493–501.
[13] Robling AG, Niziolek PJ, Baldridge LA, Condon KW, Allen MR, Alam I, et al. Mechanical stimulation of bone in vivo reduces osteocyte expression of Sost/sclerostin. J Biol Chem 2008;283:5866–75.
[14] Lambers FM, Schulte FA, Kuhn G, Webster DJ, Muller R. Mouse tail vertebrae adapt to cyclic mechanical loading by increasing bone formation rate and decreasing bone resorption rate as shown by time-lapsed in vivo imaging of dynamic bone morphometry. Bone 2011;49:1340–50.
[15] Lu Y, Thiagarajan G, Nicolella DP, Johnson ML. Load/strain distribution between ulna and radius in the mouse forearm compression loading model. Med Eng Phys 2012;34:350–6.
[16] De Souza RL, Matsuura M, Eckstein F, Rawlinson SC, Lanyon LE, Pitsillides AA. Non-invasive axial loading of mouse tibiae increases cortical bone formation and modifies trabecular organization: a new model to study cortical and cancellous compartments in a single loaded element. Bone 2005;37:810–8.
[17] Fritton JC, Myers ER, Wright TM, van der Meulen MC. Loading induces site-specific increases in mineral content assessed by microcomputed tomography of the mouse tibia. Bone 2005;36:1030–8.
[18] Weatherholt AM, Fuchs RK, Warden SJ. Cortical and trabecular bone adaptation to incremental load magnitudes using the mouse tibial axial compression loading model. Bone 2013;52:372–9.
[19] Holguin N, Brodt MD, Sanchez ME, Kotiya AA, Silva MJ. Adaptation of tibial structure and strength to axial compression depends on loading history in both C57BL/6 and BALB/c mice. Calcif Tissue Int 2013;93:211–21.
[20] Sztefek P, Vanleene M, Olsson R, Collinson R, Pitsillides AA, Shefelbine S. Using digital image correlation to determine bone surface strains during loading and after adaptation of the mouse tibia. J Biomech 2010;43:599–605.
[21] Price C, Li W, Novotny JE, Wang L. An in-situ fluorescence-based optical extensometry system for imaging mechanically loaded bone. J Orthop Res 2010;28:805–11.
[22] Stadelmann VA, Hocke J, Verhelle J, Forster V, Merlini F, Terrier A, et al. 3D strain map of axially loaded mouse tibia: a numerical analysis validated by experimental measurements. Comput Methods Biomech Biomed Engin 2009;12:95–100.
[23] Moustafa A, Sugiyama T, Prasad J, Zaman G, Gross TS, Lanyon LE, et al. Mechanical loading-related changes in osteocyte sclerostin expression in mice are more closely associated with the subsequent osteogenic response than the peak strains engendered. Osteoporos Int 2012;23:1225–34.
[24] Willie BM, Birkhold AI, Razi H, Thiele T, Aido M, Kruck B, et al. Diminished response to in vivo mechanical loading in trabecular and not cortical bone in adulthood of female C57Bl/6 mice coincides with a reduction in deformation to load. Bone 2013;55:335–46.
[25] Patel TK, Brodt MD, Silva MJ. Experimental and finite element analysis of strains induced by axial tibial compression in young-adult and old female C57Bl/6 mice. J Biomech 2014;47:451–7.
[26] Biewener AA. Biomechanics—structures and systems. Oxford University Press; 1992.
[27] Main RP, Lynch ME, van der Meulen MC. In vivo tibial stiffness is maintained by whole bone morphology and cross-sectional geometry in growing female mice. J Biomech 2010;43:2689–94.
[28] Lynch ME, Main RP, Xu Q, Schmicker TL, Schaffler MB, Wright TM, et al. Tibial compression is anabolic in the adult mouse skeleton despite reduced responsiveness with aging. Bone 2011;49:439–46.
[29] Melville KM, Kelly NH, Khan SA, Schimenti JC, Ross FP, Main RP, et al. Female mice lacking estrogen receptor-alpha in osteoblasts have compromised bone mass and strength. J Bone Miner Res 2014;29:370–9.
[30] Fang QQ, Boas DA. Tetrahedral mesh generation from volumetric binary and gray-scale images. 2009 IEEE international symposium on biomedical imaging: from nano to macro, vols. 1 and 2; 2009. p. 1142–5.

[31] Sugiyama T, Meakin LB, Browne WJ, Galea GL, Price JS, Lanyon LE. Bones' adaptive response to mechanical loading is essentially linear between the low strains associated with disuse and the high strains associated with the lamellar/woven bone transition. J Bone Miner Res 2012;27:1784–93.
[32] Cotter SC. Screening design for factorial-experiments with interactions. Biometrika 1979;66:317–20.
[33] Schuff MM, Gore JP, Nauman EA. A mixture theory model of fluid and solute transport in the microvasculature of normal and malignant tissues. II: factor sensitivity analysis, calibration, and validation. J Math Biol 2013;67:1307–37.
[34] Glatt V, Canalis E, Stadmeyer L, Bouxsein ML. Age-related changes in trabecular architecture differ in female and male C57BL/6J mice. J Bone Miner Res 2007;22:1197–207.
[35] Yang H, Ma X, Guo T. Some factors that affect the comparison between isotropic and orthotropic inhomogeneous finite element material models of femur. Med Eng Phys 2010;32:553–60.
[36] Easley SK, Jekir MG, Burghardt AJ, Li M, Keaveny TM. Contribution of the intra-specimen variations in tissue mineralization to PTH- and raloxifene-induced changes in stiffness of rat vertebrae. Bone 2010;46:1162–9.
[37] Silva MJ, Brodt MD, Hucker WJ. Finite element analysis of the mouse tibia: estimating endocortical strain during three-point bending in SAMP6 osteoporotic mice. Anat Rec A Discov Mol Cell Evol Biol 2005;283:380–90.
[38] Rieppo L, Saarakkala S, Jurvelin JS, Rieppo J. Prediction of compressive stiffness of articular cartilage using Fourier transform infrared spectroscopy. J Biomech 2013;46:1269–75.
[39] Torcasio A, Zhang X, Duyck J, van Lenthe GH. 3D characterization of bone strains in the rat tibia loading model. Biomech Model Mechanobiol 2012;11:403–10.
[40] Dodge T, Wanis M, Ayoub R, Zhao L, Watts NB, Bhattacharya A, et al. Mechanical loading, damping, and load-driven bone formation in mouse tibiae. Bone 2012;51:810–8.